Supplement of Atmos. Chem. Phys., 14, 6395–6415, 2014
http://www.atmos-chem-phys.net/14/6395/2014/
doi:10.5194/acp-14-6395-2014-supplement

Atmospheric Chemistry and Physics Open Access

Supplement of

Extensive spatiotemporal analyses of surface ozone and related meteorological variables in South Korea for the period 1999–2010

J. Seo et al.

Correspondence to: D. Youn (dyoun@chungbuk.ac.kr)

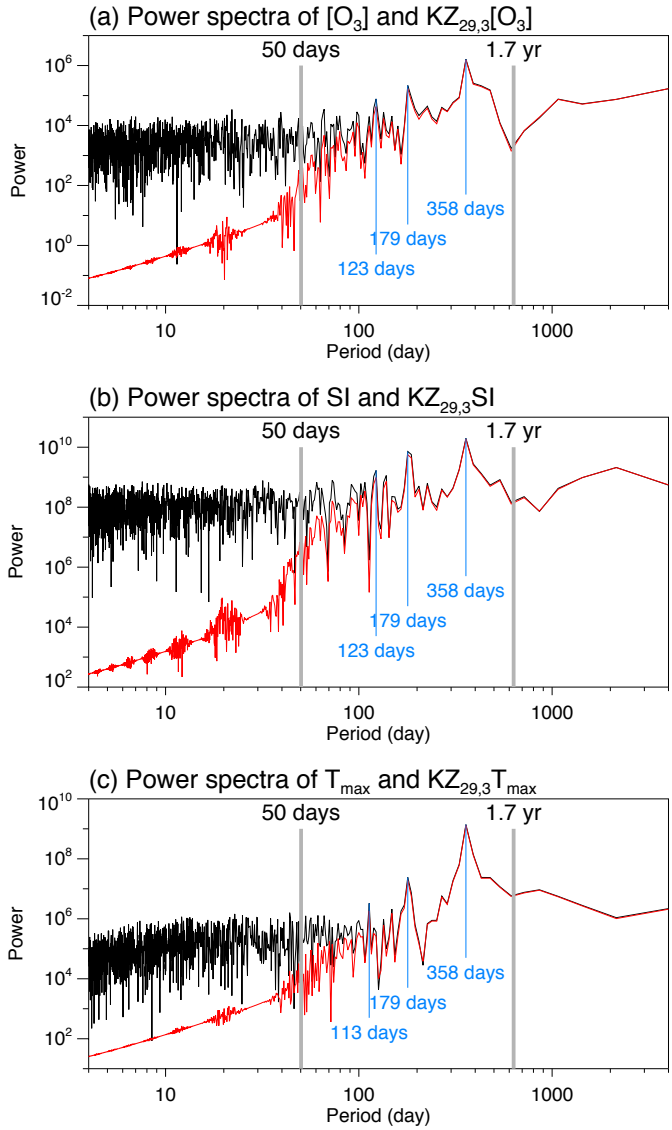

Figure S1. Power spectra of **(a)** log-transformed $O_{3\ 8h}$ time series ($[O_3]$) and its baseline ($KZ_{29,3}[O_3]$) at the City Hall of Seoul, **(b)** daily average surface insolation (SI) and its baseline ($KZ_{29,3}SI$), and **(c)** daily maximum temperature (T_{max}) and its baseline ($KZ_{29,3}T_{max}$) observed at the weather station in Seoul for the period 1999–2000. Each power spectra of original time series and its baseline obtained by $KZ_{29,3}$ filter are represented as black and red lines, respectively.

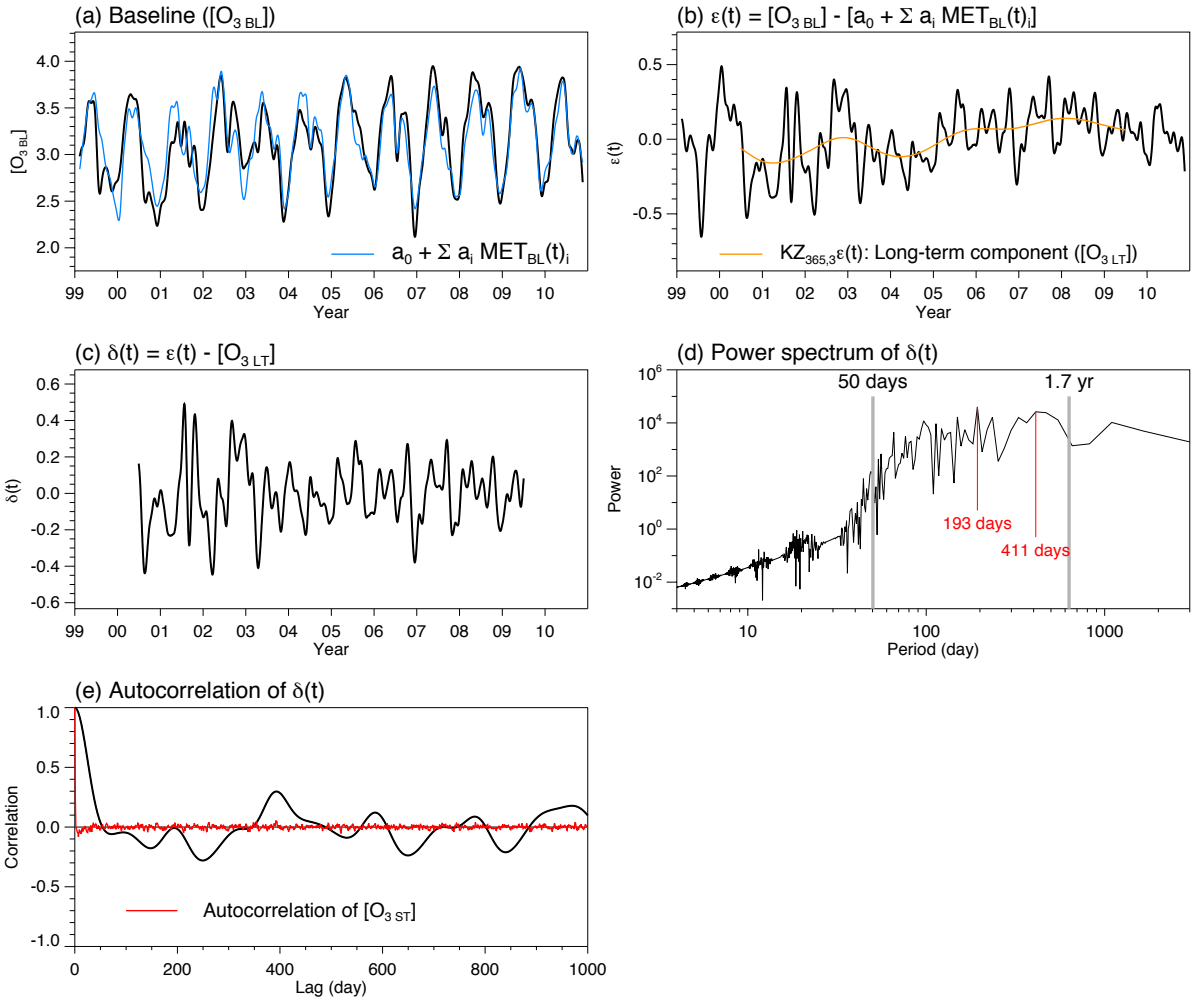

Figure S2. Time series of **(a)** baseline of log-transformed $O_{3\ 8h}$ ($[O_{3\ BL}]$) and combined meteorological variables regressed on the baseline ($a_0 + \sum_i a_i\ MET_{BL}(t)_i$), **(b)** $\varepsilon(t)$ and long-term component ($[O_{3\ LT}]$), and **(c)** $\delta(t)$ at the City Hall of Seoul. **(d)** Power spectrum of $\delta(t)$. **(e)** Autocorrelation of $\delta(t)$ and short-term component ($[O_{3\ ST}]$).

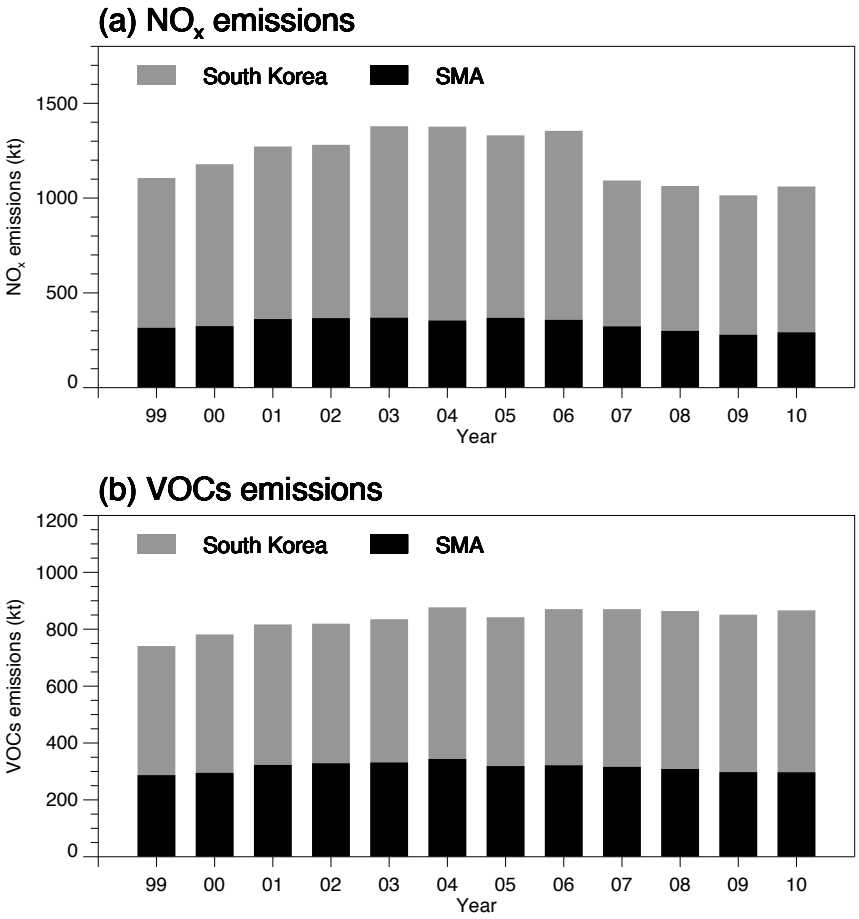

Figure S3. Total anthropogenic emissions of **(a)** NOx and **(b)** VOCs in the SMA and in South Korea (KMOE, 2013). It should be noted that the rapid decrease in NO_x emissions between the years 2006 and 2007 mainly results from applying different assessment method to the NO_x emissions from the energy industry before and after 2007.

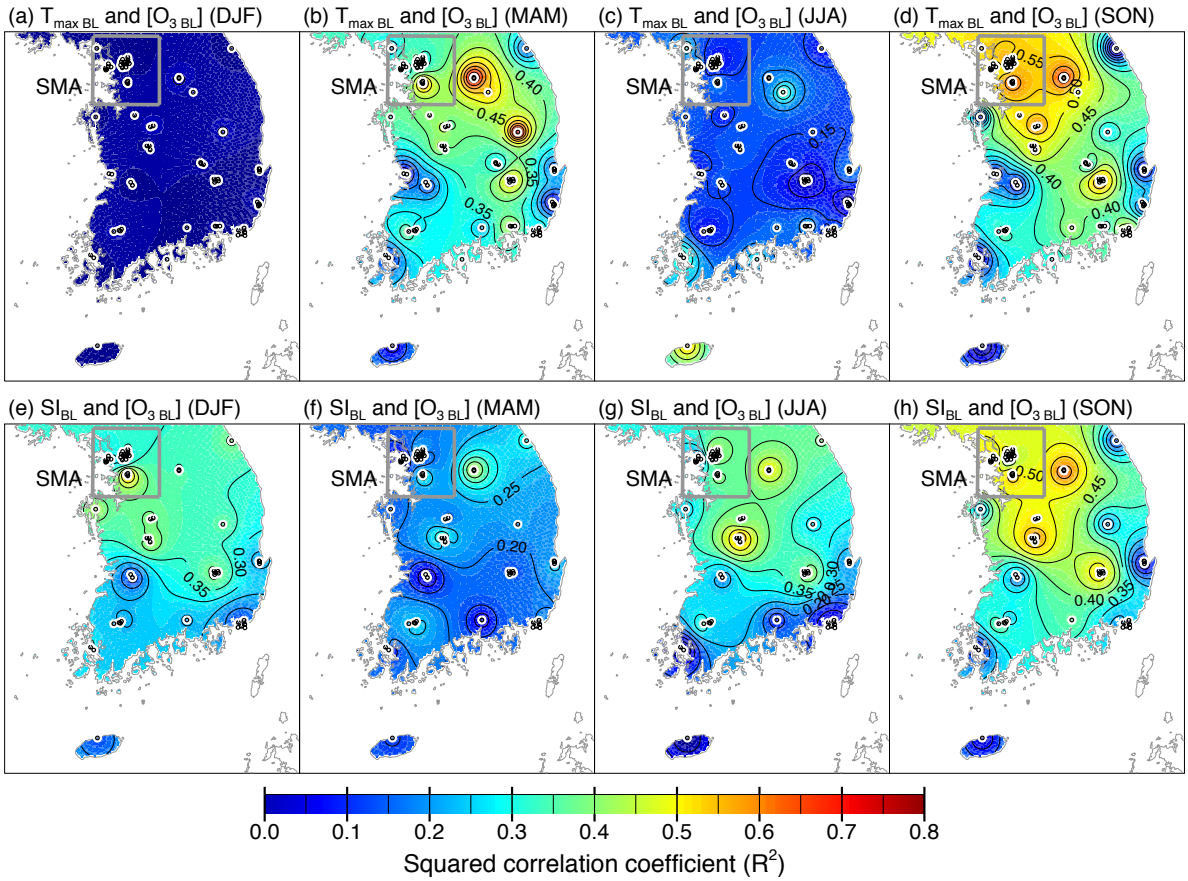

Figure S4. Spatial distributions of R^2 between baselines of $O_{3\ 8h}$ ($[O_{3\ BL}]$) and daily maximum temperature ($T_{max\ BL}$) in **(a)** winter, **(b)** spring, **(c)** summer, and **(d)** autumn, and R^2 between $[O_{3\ BL}]$ and daily average insolation (SI_{BL}) during **(e)** winter, **(f)** spring, **(g)** summer, and **(h)** autumn for the period 1999–2010.

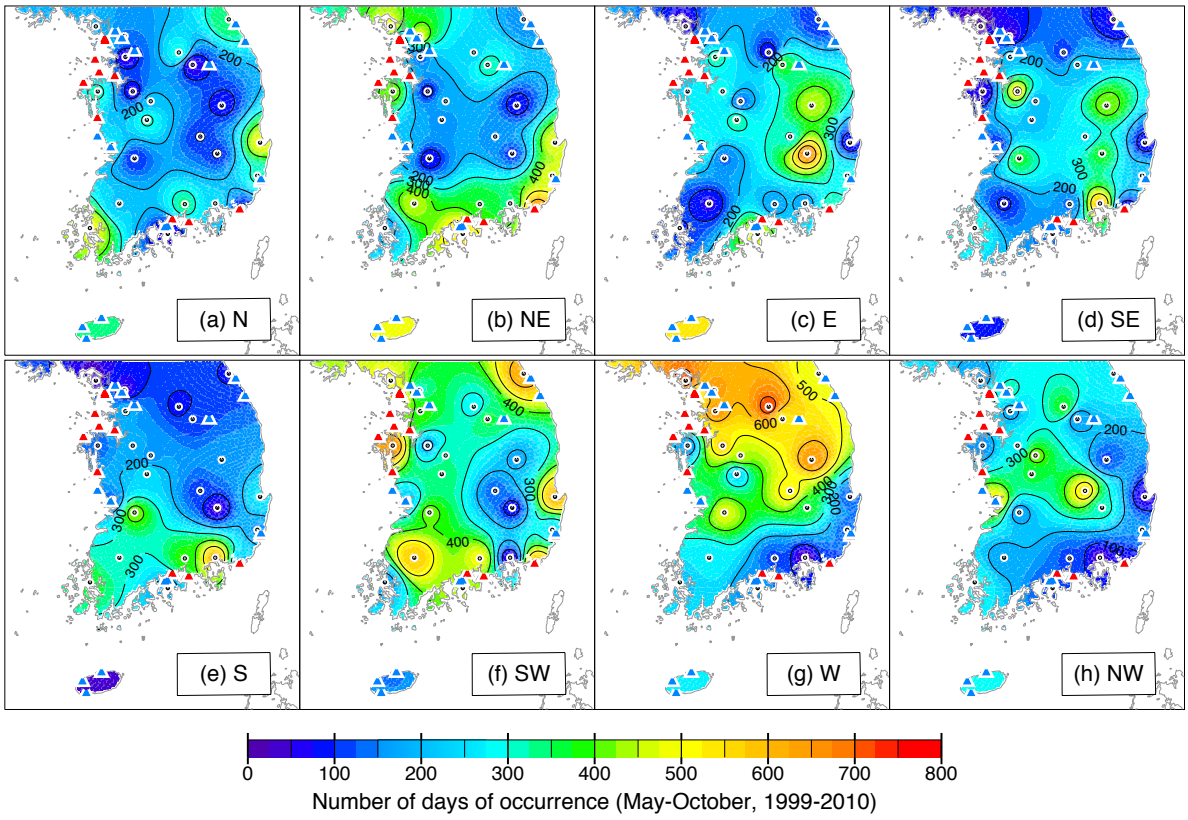

Figure S5. Spatial distributions of number of days in each wind direction (WD) during the months of frequent high O_3 events (May–October) for the period 1999-2010.

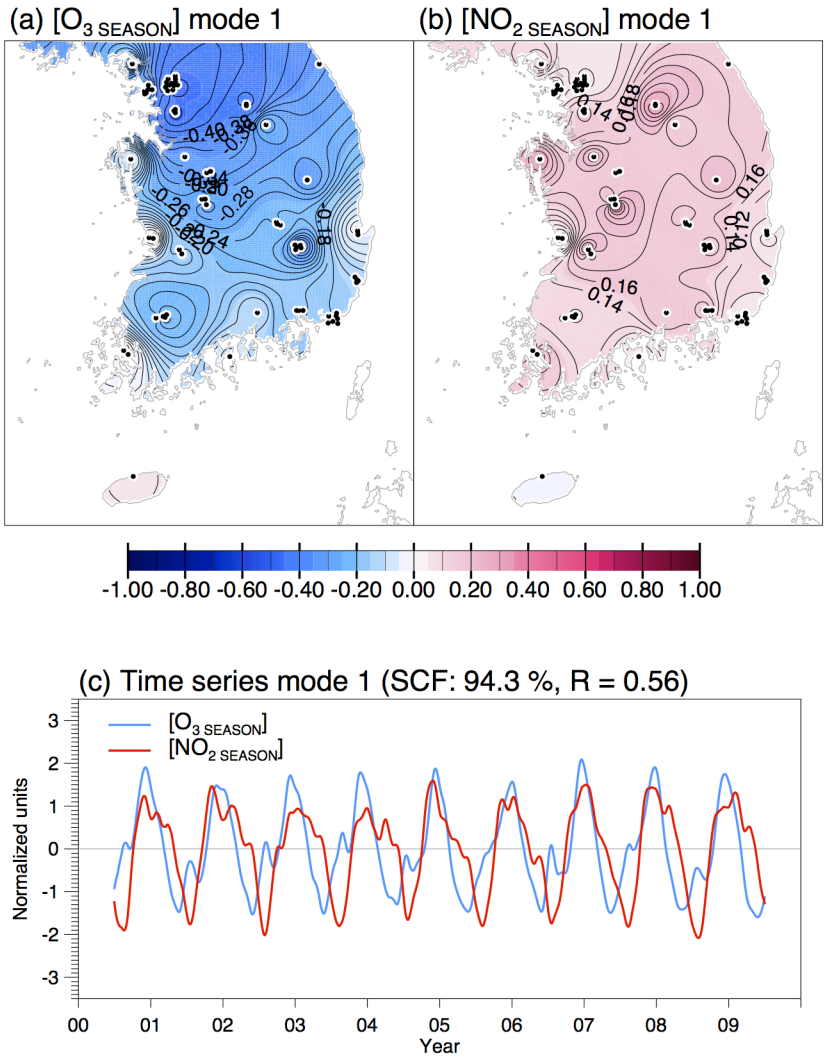

Figure S6. The first leading mode of SVD between the seasonal components of **(a)** daily maximum 8-h average O_3 ([O_3 SEASON]) and **(b)** daily average NO_2 ([NO_2 SEASON]) with **(c)** time series of the SVD expansion coefficient associated with [O_3 SEASON] mode (blue line) and [NO_2 SEASON] mode (red line).

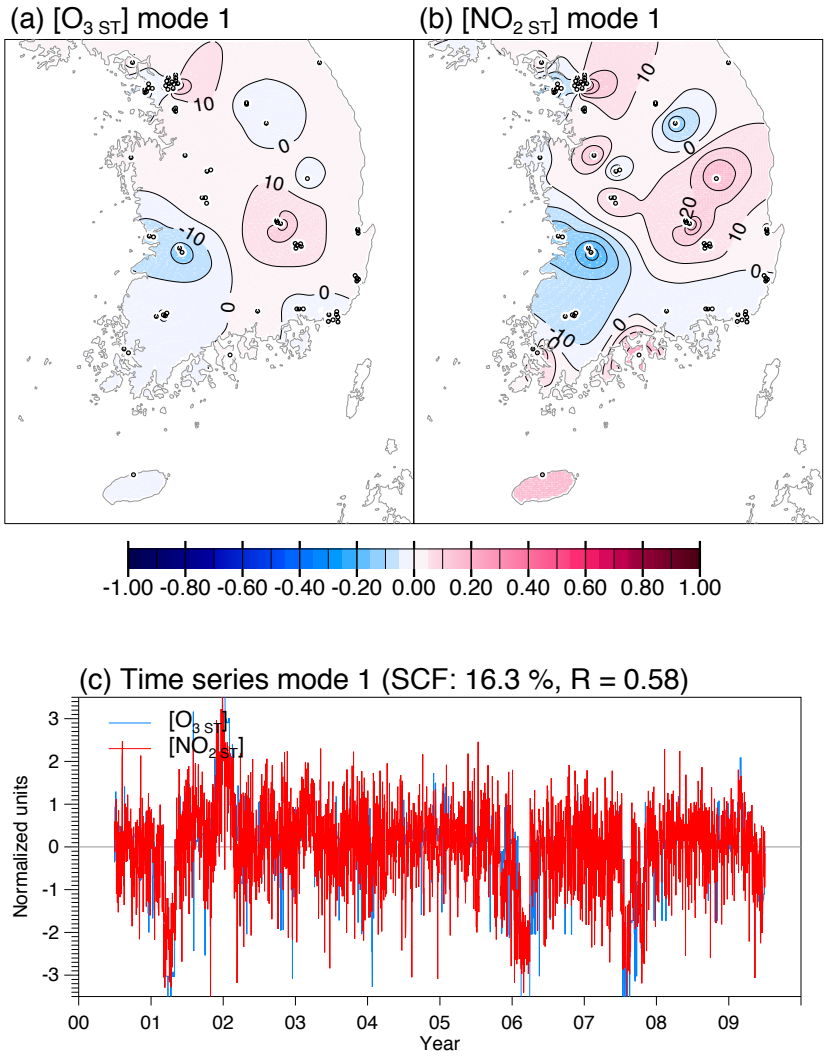

Figure S7. The first leading mode of SVD between the short-term components of **(a)** daily maximum 8-h average O_3 ($[O_{3\ ST}]$) and **(b)** daily average NO_2 ($[NO_{2\ ST}]$) with **(c)** time series of the SVD expansion coefficient associated with $[O_{3\ ST}]$ mode (blue line) and $[NO_{2\ ST}]$ mode (red line).

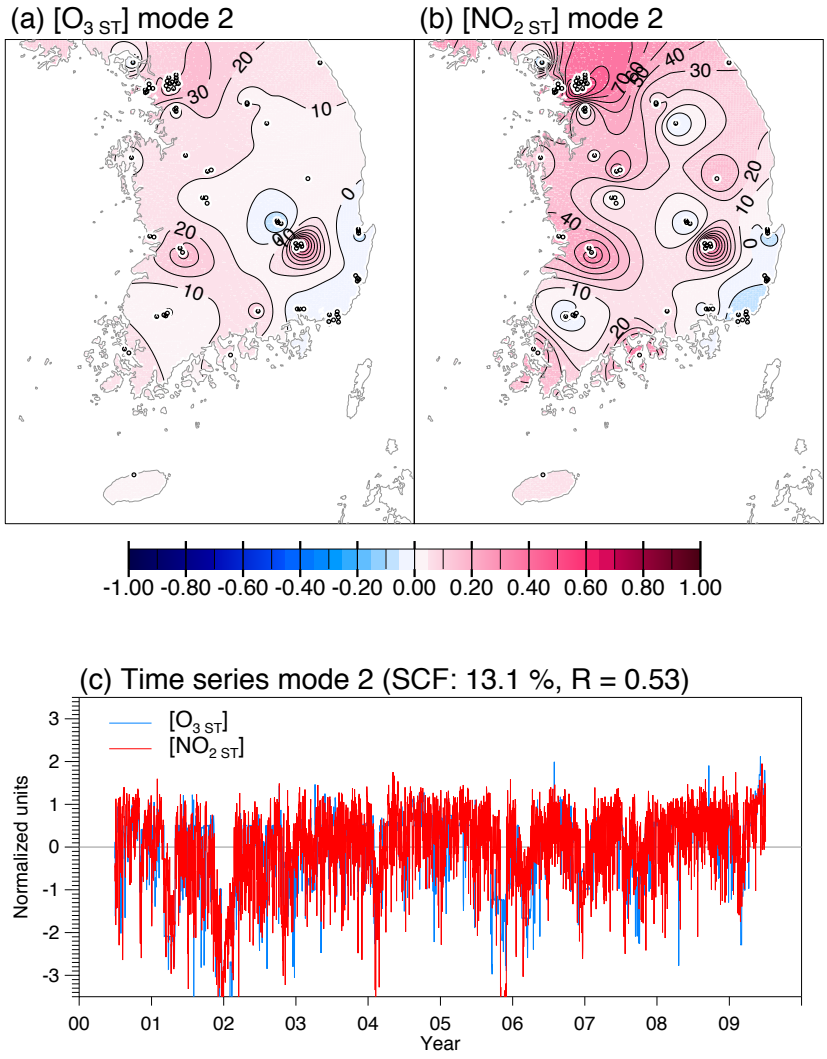

Figure S8. The second mode of SVD between the short-term components of **(a)** daily maximum 8-h average O_3 ($[O_{3\ ST}]$) and **(b)** daily average NO_2 ($[NO_{2\ ST}]$) with **(c)** time series of the SVD expansion coefficient associated with $[O_{3\ ST}]$ mode (blue line) and $[NO_{2\ ST}]$ mode (red line).